

We are IntechOpen, the world's leading publisher of Open Access books Built by scientists, for scientists

6,900

Open access books available

186,000

International authors and editors

200M

Downloads

Our authors are among the

154

Countries delivered to

TOP 1%

most cited scientists

12.2%

Contributors from top 500 universities



WEB OF SCIENCE™

Selection of our books indexed in the Book Citation Index
in Web of Science™ Core Collection (BKCI)

Interested in publishing with us?
Contact book.department@intechopen.com

Numbers displayed above are based on latest data collected.
For more information visit www.intechopen.com



Simulation of Dynamic Recrystallization in Solder Interconnections during Thermal Cycling

Jue Li, Tomi Laurila, Toni T. Mattila, Hongbo Xu and Mervi Paulasto-Kröckel

Additional information is available at the end of the chapter

<http://dx.doi.org/10.5772/53820>

1. Introduction

Solder alloys are widely used bonding materials in electronics industry. The reliability concerns for solder interconnections, which provide both mechanical and electronic connections, are rising with the increasing use of highly integrated components in portable electronic products [1-6]. As shown in Fig. 1, a typical ball grid array (BGA) component board usually consists of a silicone die, molding compound, solder interconnections, and printed wiring board (PWB). In service, all products are subjected to thermal cycles as a result of temperature changes due to component internal heat dissipation or ambient temperature changes. The existence of coefficient of thermal expansion (CTE) mismatches between dissimilar materials (about 16 ppm/°C for PWB and 2.5 ppm/°C for Si die [7]) is the source of deformation and thermomechanical stress in the solder interconnection, which leads to the cracking of the interconnections and failures of the electronic devices.

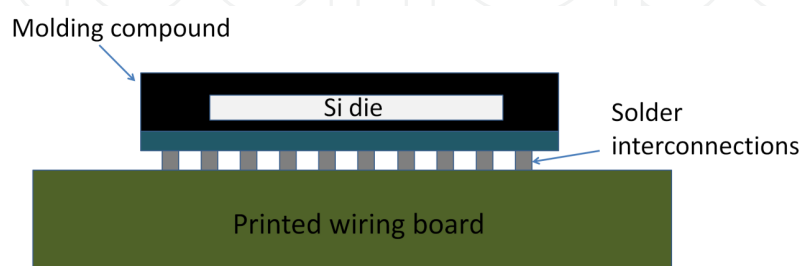


Figure 1. Schematic show of a typical BGA component board.

Since failure of solder interconnections is a typical failure mode in many electronic devices, the reliability and life time prediction of solder interconnections become crucial. Various reliability test and computer-aided simulations have been carried out to study the solder interconnection reliability [8-17]. With the experimental and simulation results, a number of lifetime prediction models have been established and they can be classified into two main categories: strain-based and energy-based. For instance, the Engelmaier model is based on the total shear strain range, the Coffin-Manson model on the plastic strain, and the Darveaux model on the energy density [18-20]. However, microstructural changes in the bulk solder have not yet been included in any of the popular prediction models. Especially the microstructural changes associated with recrystallization and grain growth are of importance because they can significantly affect the mechanical properties and can cause recrystallization induced failure of solder interconnections [21-26]. A new approach for lifetime prediction needs to be developed that takes into account the microstructural changes. In order to achieve this, the first step is to quantitatively study the recrystallization and grain growth occurring in solder interconnections.

In this chapter, the current understanding of the microstructural changes in solder interconnections is introduced, followed by a brief review of the Monte Carlo simulations of grain growth and recrystallization. Then, a new algorithm for predicting dynamic recrystallization in solder interconnections during thermal cycling tests is presented.

2. Microstructural changes of Sn-rich solder interconnections

The microstructure of a solder alloy has a very significant effect on its material properties. A brief introduction of the microstructural changes of tin (Sn) rich solder interconnections is addressed in this section. With the implementation of lead (Pb) free technology in microelectronics [27], tin based lead-free solder alloys have replaced the traditional SnPb alloys. Currently, the three-component tin-silver-copper (SnAgCu) alloy with near-eutectic composition is the most widely used solder alloy. For simplicity, the following microstructural study focuses on one solder alloy with the composition Sn3.0Ag0.5Cu.

2.1. As-solidified microstructures of Sn-rich solder interconnections

After reflow the solder interconnections normally consist of relatively few solidification colonies (less than five) [28]. Micrographs of a typical as-solidified SnAgCu solder interconnection are presented in Fig. 2. The boundaries between the contrasting areas, as seen in polarized light image in Fig. 2b are high-angle boundaries (larger than 15°) between matrices of solidification colonies composed of Sn cells and Cu_6Sn_5 and Ag_3Sn particles. Within the colony boundaries, a uniformly oriented cellular solidification structure of tin is enclosed [29-33]. The cellular structure of tin is clearly distinguishable as cells are surrounded by eutectic regions. Besides the cellular structure, there are also some large Cu_6Sn_5 and Ag_3Sn bulk intermetallic compound (IMC) precipitates.

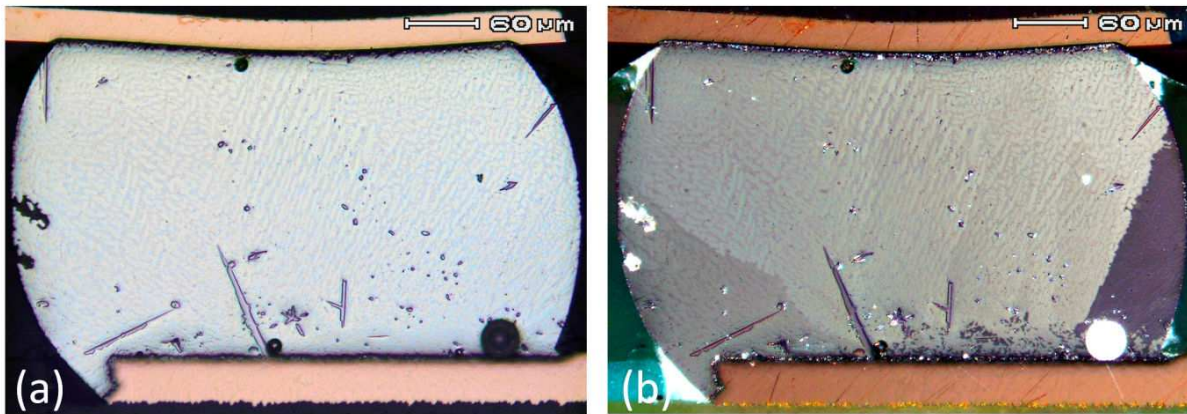


Figure 2. The as-solidified microstructure of a SnAgCu solder interconnection; (a) optical bright field image, (b) cross-polarized light image.

2.2. Recovery and recrystallization of Sn-rich solder interconnections

For decades, the industry has used recrystallization to control microstructures, and static recrystallization of structural metals after deformation is probably the best understood recrystallization process [22]. On the other hand, dynamic recrystallization during cyclic deformation, which occurs in solder interconnections, has received much less attention and is still poorly understood. This is because the related microstructural events are highly complex from the microstructural point of view. The major understanding of this subject is briefly summarized as follows.

Thermal cycling tests with extreme temperatures in the range of about $-40\text{ }^{\circ}\text{C}$ to $+125\text{ }^{\circ}\text{C}$ are usually carried out to assess the reliability of electronic devices [35, 36]. During thermal cycling, the solder interconnections are under cyclic loading conditions. The induced thermo-mechanical stresses are often higher than the yield strength of the material, which leads to plastic deformation. A fraction of the energy associated with the plastic deformation of solder interconnections is stored in the metal, mainly in the form of dislocations. The stored energy is subsequently released during restoration, which can be divided into three main processes: recovery, primary recrystallization and grain growth. Recovery and recrystallization are two competing processes, which are driven by the increased internal energy of the deformed solder. Recovery decreases the driving force for recrystallization and thus hinders the initiation of recrystallization. In high stacking fault energy metals such as Sn, the release of stored energy takes place so effectively by recovery that recrystallization will not practically take place [22, 23]. Studies have shown that after a single deformation static recrystallization rarely occurs in Sn-rich solders [37]. However, under dynamic loading conditions such as in thermal cycling tests, recrystallization often takes place in the high stress concentration regions of solder interconnections [28, 38, 39].

Experimental observations indicate that the microstructure of solder interconnections may change significantly during thermal cycling tests. The as-solidified microstructure can trans-

form locally into a more or less equiaxed grain structure by recrystallization. An example is presented in Fig. 3 where the cross-section images of a solder interconnection after 6000 thermal cycles are shown. Part of the solder interconnection was recrystallized near the component side after 6000 thermal cycles (see Fig. 3b). It is noteworthy that optical microscopy with polarized light shows the areas of different orientations with different colors and it is an excellent tool for observing the recrystallized region. In the recrystallized region a continuous network of high angle grain boundaries provides favorable sites for cracks to nucleate and to propagate intergranularly, which can lead to an early failure of the component. This kind of failure mode is regarded as the recrystallization-assisted cracking. More details can be found in the references [14, 26, 28].

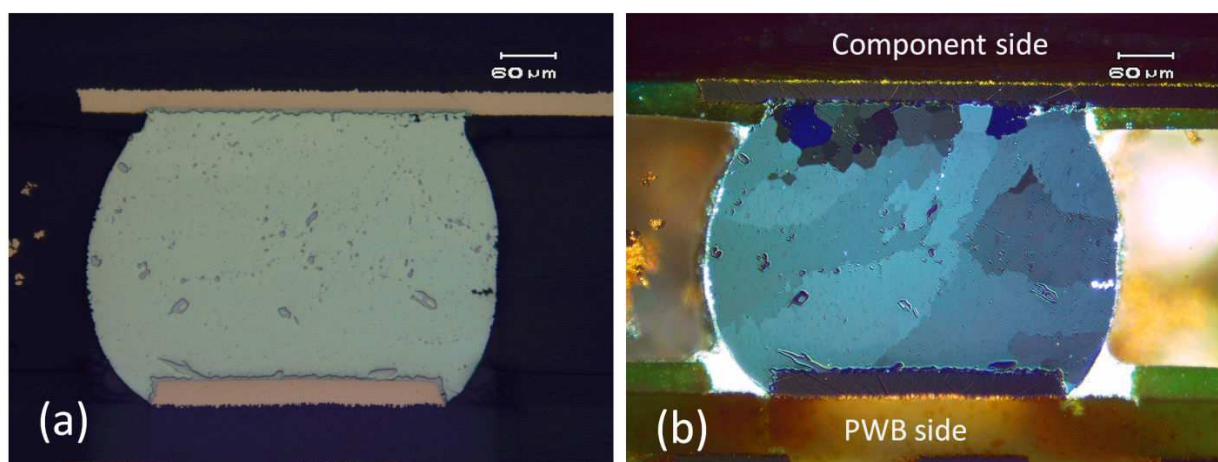


Figure 3. Micrographs of the solder interconnection after 6000 thermal cycles; (a) optical bright field image, (b) cross-polarized light image.

2.3. Effect of intermetallic compound precipitates

In the near-eutectic SnAgCu alloys, mainly two kinds of IMC precipitates, Cu_6Sn_5 and Ag_3Sn , can form upon solidification. The size of intermetallic particles (IMPs) varies a lot: the small and finely distributed IMPs are located at the boundaries of tin cells (eutectic structure) while the relatively large IMPs are randomly distributed in the bulk solder. Fine particles usually prevent the motion of grain boundaries by exerting a pinning force, and therefore, suppress the progress of recrystallization. The influence of fine particles on recrystallization has been studied in earlier work, e.g. [40]. It is believed that fine particles do not remarkably affect the distribution of stored energy within the grains. However, coarse particles exert localized stress and strain concentrations due to the mismatch of mechanical properties and thermal expansion coefficients during thermal cycling. Dislocation density is increased in the particle-affected deformation regions, which provide favorable sites for nucleation of recrystallization.

3. Monte Carlo simulations

Many models have been developed to simulate microstructural evolution, such as vertex model, Monte Carlo (MC) Potts model, phase field model, and cellular automata (CA) model [22, 23, 41, 42]. For modeling recrystallization, the MC Potts model and CA model are perhaps the two most popular candidates. In general, the MC Potts model and CA model are similar to each other since both models include a lattice, use discrete orientations and describe stored energy in terms of a scalar stored energy term. The MC Potts model provides a convenient way to simulate the changes in microstructures and it has been successfully applied to simulate the recrystallization process in solder interconnections as well as in many other applications, e.g. [38, 39, 43-45].

3.1. Monte Carlo simulation of grain growth

The MC grain growth simulation originates from Ising and Potts models for magnetic domain evolution [46]. The Ising model consists of two spin states, namely up and down, and the Potts model allows multiple states (Q states) for each particle in the system. The Potts model has been widely used for modeling material behaviors, such as grain growth and texture evolution, e.g. [47-49].

During the MC grain growth simulation, a continuum microstructure is mapped onto a 2D MC lattice, which can be either triangular or rectangular lattice [50]. In order to initialize the lattice, an integer number S_i (between 1 and Q) is assigned to each lattice site, where Q represents the total number of orientations in the system. Two adjacent sites with different grain orientation numbers are regarded as being separated by a grain boundary and each pair of unlike neighboring sites contributes a unit of grain boundary energy, J , to the system. A group of sites having the same orientation number and surrounded by grain boundaries are considered as a grain. The total energy of the system, E , is calculated by the grain boundary energy contributions throughout all the sites.

$$E = J \sum_{\langle ij \rangle} (1 - \delta_{S_i S_j}) \quad (1)$$

where the sum of i is over all N_{MC} sites in the system, the sum of j is over all the nearest-neighbor sites of the site i , and δ_{ij} is the Kronecker delta.

The Monte Carlo method iteratively simulates the grain growth process by the following key steps [51-53].

- a. Choose a lattice site i in random
- b. If the selected site is an interior site, no reorientation will be tried. Go back to 'step a'
- c. If the selected site is at the grain boundary, its neighboring sites are checked. Assign a new orientation number to the site. The new orientation is limited to those orientations of the neighboring grains, and is weighted by the number of neighbors with the same orientation

- d. Calculate the energy change ΔE associated the site orientation change
- e. If ΔE is non-positive, the attempted reorientation is accepted, otherwise, the old orientation of the site is recovered
- f. Increment time regardless of whether the reorientation attempt is accepted or not
- g. Go to 'step a' until the end of the simulation

3.2. Monte Carlo simulation of recrystallization

The major differences between the simulation of recrystallization and grain growth are the bulk stored energy and the nucleation process. A fraction of the energy associated with the deformation of material is stored in the metal, mainly in the form of dislocations. The distribution of stored energy is heterogeneous, and therefore each site contributes an amount of stored energy, $H(S_i)$, to the system. The total energy of the system, E , is calculated by summing the volume stored energy and the grain boundary energy contributions throughout all the sites.

$$E = J \sum_{\langle ij \rangle} (1 - \delta_{S_i S_j}) + \sum_i H(S_i) \quad (2)$$

In static recrystallization simulations, the stored energy of each site is positive for unrecrystallized sites and zero for recrystallized sites. However, in the case of dynamic recrystallization the stored energy is a function of both time and position as new energy is added to the lattice continuously.

The nucleation process is modeled by introducing nuclei (small embryos with zero stored energy) into the lattice at random positions. Embryos have orientations that differ from all the other grains of the original microstructure. Embryos can be added to the lattice at the beginning of the simulation or at a regular interval during the simulation. In the reorientation process, if the randomly selected site is unrecrystallized, it will be recrystallized under the condition that the total energy of the system is reduced. If the selected site is recrystallized, the reorientation process is a simulation of the nucleus growth process or the grain growth process.

3.3. Monte Carlo simulation of recrystallization with the presence of particles

The particles are normally introduced to the MC sites at the beginning of the simulation, and those sites have an orientation different from any other grains. The particles do not react, dissolve or grow during the simulation, and thereby are named as inert particles [50]. These assumptions have been proved to be effective, especially for small particles. However, the influence on nucleation stimulation should be considered for large particles. Large particles exert localized stress and strain concentrations and cause the increase of dislocation density in the particle-affected deformation regions, which provide favorable sites for nucleation of recrystallization.

4. Multiscale simulation algorithms

The treatment of heterogeneous nucleation and inhomogeneously deformed material remains a challenge for the MC method. Hybrid methods are needed to perform the task. As steps in this direction, Rollett et al. developed a hybrid model for mesoscopic simulation of recrystallization by combining the MC and Cellular Automaton methods [43]. Song et al. presented a hybrid MC model for studying recovery and recrystallization of titanium at various annealing temperatures after inhomogeneous deformation [44]. Yu et al. combined the MC method with the finite element (FE) method in order to simulate the microstructure of structural materials under forging and rolling [45]. However, most of the early studies are about the simulations of static recrystallization. Recently, Li et al. presented a hybrid algorithm for simulating dynamic recrystallization of solder interconnections during thermal cycling [38, 39].

The details of the multiscale simulation of dynamic recrystallization of solder interconnections are presented as follows. The finite element method is utilized to model macroscale inhomogeneous deformation, and the Monte Carlo Potts model is utilized to model the mesoscale microstructural evolution. Compared to the in situ experimental observations, a correlation between real time and MC simulation time is established. In addition, the effects of intermetallic particles (Cu_6Sn_5 and Ag_3Sn) on recrystallization in solder matrix are included in the simulation.

4.1. Thermal cycling test and model assumptions

Thermal cycling (TC) tests are accelerated fatigue tests, which subject the components and solder interconnects to alternating high and low temperature extremes [35, 36]. The tests are conducted to determine the ability of the parts to resist a specified number of temperature cycles from a specified high temperature to a specified low temperature with a certain ramp rate and dwell time. A typical temperature profile for a TC test is shown in Fig. 4.

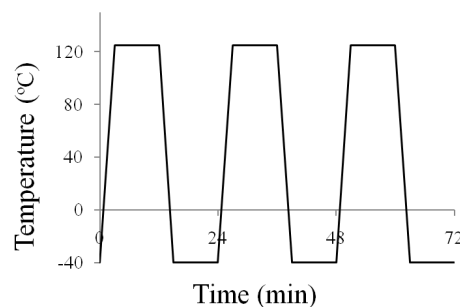


Figure 4. A typical temperature profile with temperature range from $-40\text{ }^{\circ}\text{C}$ to $125\text{ }^{\circ}\text{C}$, with a 6 minute ramp time and an 18 minute dwell time.

Each thermal cycle can be regarded as ‘deformation + annealing’ and TC tests normally last several thousand cycles before failures of the solder interconnections are detected. The algo-

rithm of dynamic recrystallization is based on the principle that the stored energy of solder is gradually increased during each thermal cycle. Even though recovery consumes a certain amount of the energy, the net change of the energy is always assumed to be positive due to the fact that newly recrystallized grains appear after a certain number of thermal cycles. When a critical value of the energy is reached, recrystallization is initiated. The stored energy is released through the nucleation and growth of new grains, which gradually consume the strain-hardened matrix of high dislocation density.

4.2. Multiscale simulation process

In order to schematically describe the simulation process, a flow chart is shown in Fig. 5. There are three major steps and all the key inputs for the simulation are listed in the boxes, which are on the left side of each step. In Step I, the finite element method is employed to calculate the inelastic strain energy density of the solder interconnections under thermal cycling loads. As discussed above, it is assumed that the net increase of the stored energy takes place after every thermal cycle. In Step II (scaling processes), the stored energy, as the driving force for recrystallization, is mapped onto the lattice of the MC model, and moreover, a correlation is established to convert real time to MC simulation time with the help of the in situ test results. In Step III, the grain boundary energy and the volume stored energy are taken into consideration in the energy minimization calculations to simulate the recrystallization and grain growth processes. Furthermore, intermetallic particles are treated as inert particles and their influence on the distribution of stored energy is included.

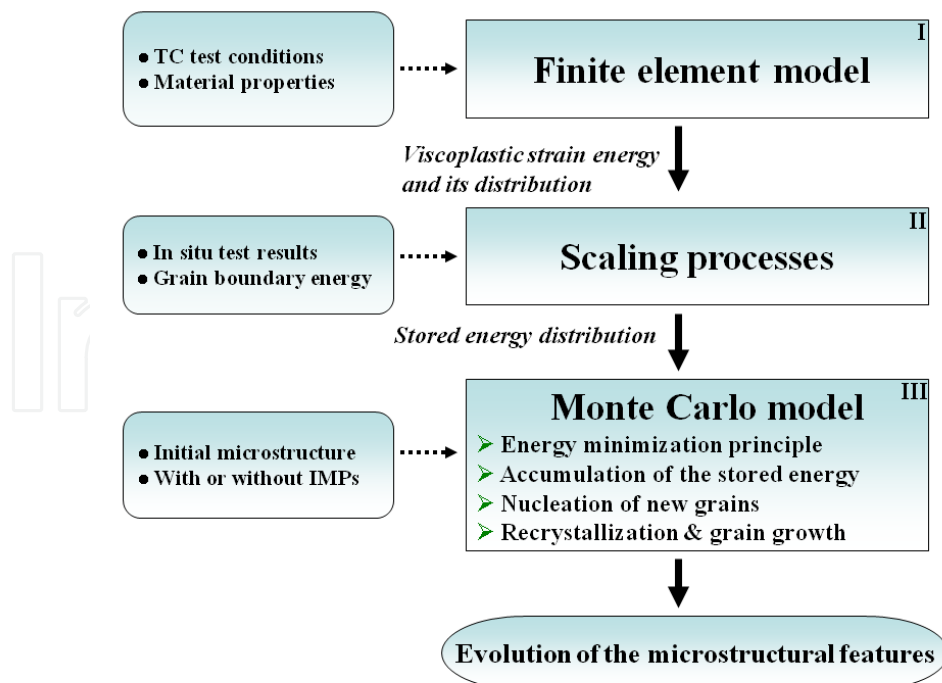


Figure 5. Flow chart for the simulation of microstructural changes in solder interconnections [39].

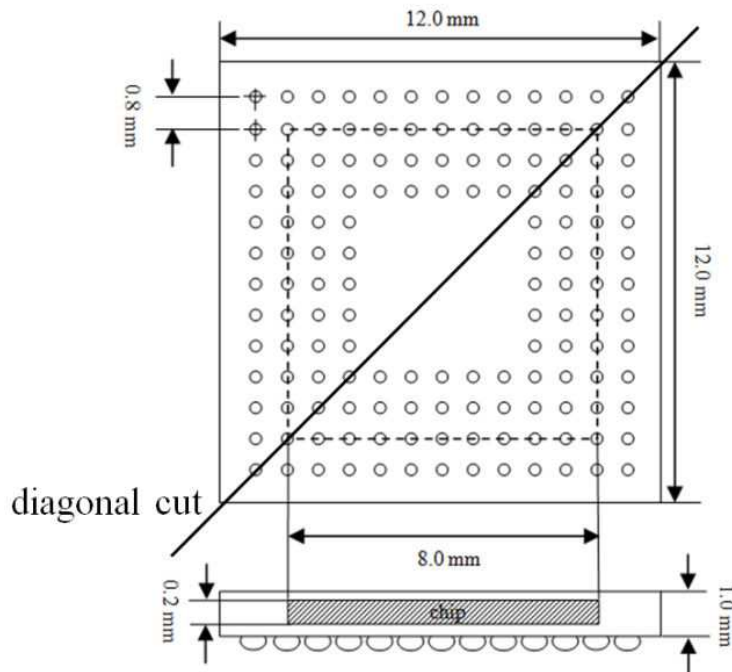


Figure 6. Schematic show of the BGA component under study [39].

4.3. Finite element model

The 3-D finite element analysis (FEA) was performed with the help of the commercial finite element software ANSYS v.12.0. The model was built up according to the experimental set-up where the ball grid array (BGA) components were cut along the diagonal line before the in situ test. A schematic drawing of the BGA component is shown in Fig. 6.

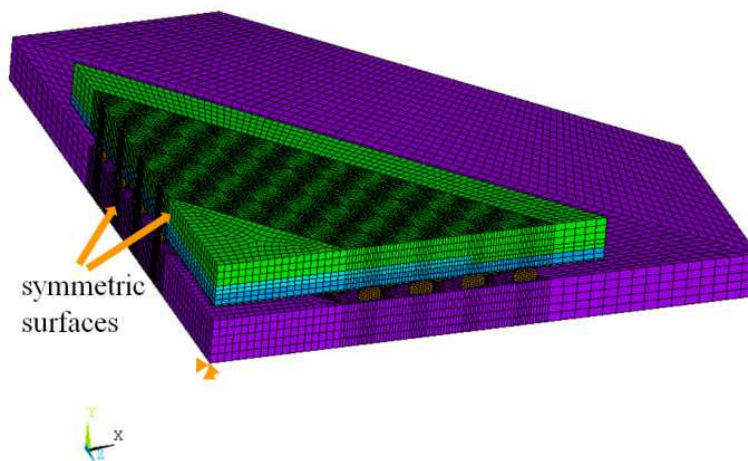


Figure 7. Finite element model for the thermomechanical calculation [39].

Symmetrical design of the component board enabled the employment of the one-fourth model of the package during FE calculation (see Fig. 7). The symmetry boundary conditions were applied to the symmetric surfaces as mechanical constraints, and the central node of the bottom of the PWB was fixed to prevent rigid body motion. Each solder interconnection was meshed with 540 SOLID185 elements as SOLID185 has plasticity, viscoplasticity, and large strain capabilities. The rest of the model was meshed with SOLID45 elements. The total number of nodes and elements of the model was 158424 and 134379, respectively. The SnAgCu solder was modeled by Anand's constitutive model with the parameters provided by Reinikainen et al. [54]. The Anand model is often used for modeling metals' behaviors under elevated temperature when the behaviors become very sensitive to strain rate, temperature, history of strain rate and temperature. The model is composed of a flow equation and three evolution equations that describes strain hardening or softening during the primary stage of creep and the secondary creep stage [55]. The inelastic strain energy is calculated by the integral of the stress with respect to the plastic strain increment.

4.4. In situ experiments

The in situ thermal cycling tests were carried out for the verifications. During the tests, the components were taken out of the test vehicle after every 500 cycles. The solder interconnections were repolished, examined, and then put back to the test vehicle to continue the test. The microstructures of the solder cross sections were examined by optical microscopy with polarized light, which shows the areas of different orientations with different colors (see Fig. 8). The boundaries between the areas of different contrast are the high angle grain boundaries. Fig. 8 (a) and Fig. 8 (b) present the typical microstructures of an outermost solder interconnection after solidification and after 1000 in situ thermal cycling test respectively, and Fig. 8 (c) is the close-up view of the recrystallized region. The dashed rectangle in Fig. 8 (b) shows the domain for the microstructural simulations.

4.5. Scaling processes

Generally speaking, there is no physically meaningful time and length scale in MC simulation, and therefore, it is difficult to compare the simulation results to experimental observations. Some calibration procedures are necessary in order to establish a relationship between real time and MC simulation time. Furthermore, the calculated inelastic strain energy needs to be converted to stored energy via a scaling process before being mapped onto the MC lattice. In the following, length scaling, time scaling and energy scaling are addressed respectively.

4.5.1. Length scaling

MC simulation does not model the behavior of single atoms and accordingly is performed at the mesoscale level. An MC lattice site represents a large cluster of atoms with the typical size being in the order of micrometers. The domain of the 2-D MC simulation covers the chosen region, which belongs to the cross section of the solder interconnection. For instance,

the size of the MC domain in this case is a 200×200 square lattice, which covers the $185 \times 185 \mu\text{m}^2$ region. Thus, the unit boundary length of the MC model, s , equals $0.925 \mu\text{m}$.

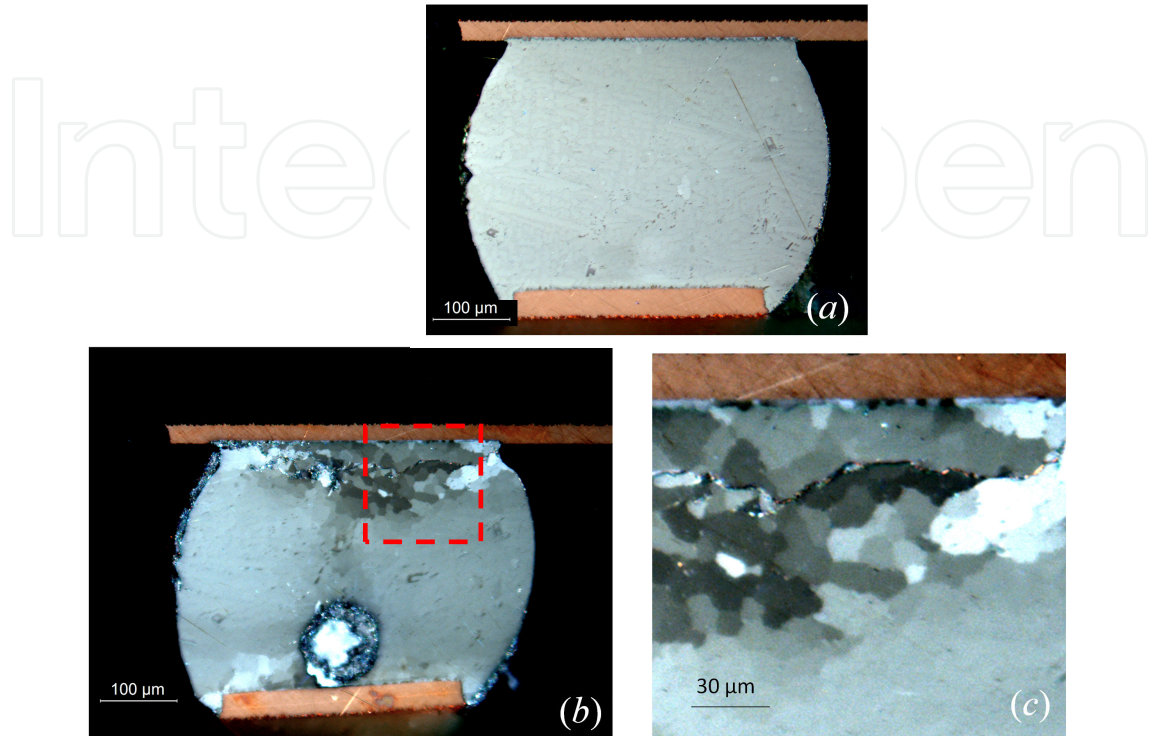


Figure 8. Microstructure of the outermost solder interconnection observed with polarized light (a) after solidification, (b) after 1000 thermal cycles observed with polarized light, (c) close-up view of the top right corner of the cross section [39].

4.5.2. Time scaling

One Monte Carlo time step (MCS) is defined as N_{MC} reorientation attempts, where N_{MC} is the total number of sites in the MC lattice. This means that each site is given an opportunity to change its orientation. A correlation between the simulation time t_{MC} [MCS] and real time t [s] is usually expressed in the following form including an apparent activation energy factor (Q_m) as well as an atomic vibration frequency (around 10^{13} Hz).

$$t_{MC} = v \exp\left(-\frac{Q_m}{RT}\right)t \quad (3)$$

where R is the universal gas constant, T is the temperature, and t is the time.

However, this time scaling process is not employed in the current study due to three main concerns. Firstly, the value of activation energy factor (Q_m) for tin is seldom reported in the literatures. Secondly, the time scaling is extremely sensitive to the value of Q_m . As shown in

Table 1, a possible error of Q_m (within the range from 20 to 107 kJ/mole) leads to a significant difference in time scale, which will finally result in unreliable simulation results. Thirdly, during each thermal cycle, the temperature alternates between a low temperature and a high temperature (e.g. from -40 °C to 125 °C, see Fig. 1), which makes it difficult to use Eq. (3).

Q_m (kJ/mole)	20	40	64	70	90	107
t_{MC}/t (MCS/s)	1.9e+10	4.7e+7	3.3e+4	5.4e+3	1.3e+1	7.5e-2

Table 1. Time scales with different activation energy factors

Besides the scaling approach in Eq. (3), other real time scaling approaches have also been developed and successfully applied to various applications. For instance, Safran et al. [56] set the time scale by multiplying the transition probability with a basic attempt frequency, and Raabe [57] scaled the real time step by a rate theory of grain boundary motion.

In order to improve both the accuracy and the efficiency, a new correlation between the simulation time t_{MC} [MCS] and real time t [TC] is established as follows.

$$t_{MC} = \frac{c_1}{c_2} t \quad (4)$$

where c_1 and c_2 are model parameters with the units [MCS] and [TC], respectively.

One thermal cycle is defined as the unit of time instead of using seconds. In this way, the relatively complicated temperature change within a thermal cycle is simplified and included only in the FE simulation and not in the MC simulation. The physical meaning of c_1 is the number of Monte Carlo time steps required for the growth of the newly recrystallized grains during each simulation time interval (STI). A certain amount of external energy is added to the MC lattice at the beginning of each STI and the amount of energy is calculated according to a certain number of thermal cycles, i.e. c_2 . Therefore, the parameter c_2 can be considered as a time compression factor and the number of simulation time intervals is equal to t/c_2 .

A series of numerical experiments were carried out and the simulated microstructures were compared to Fig. 8 (c) in order to decide the suitable model parameters, c_1 and c_2 , in Eq. 4 for the time scaling process. In theory, the value of the time compression factor, c_2 , can range from 1 to N_{TC} where N_{TC} is the total number of thermal cycles. A larger value of c_2 leads to a more efficient calculation with less accuracy. One extreme case is when c_2 equals N_{TC} and then, there will be only one simulation time interval and the process will be similar to a static recrystallization simulation. Considering efficiency and accuracy, c_2 was assumed to be 100 thermal cycles, making 10 simulation time intervals for the case $N_{TC} = 1000$. Besides c_2 , a number of different c_1 were studied. The microstructures of several typical values of c_1 are shown in Fig. 9. A small value of c_1 , e.g. $c_1 = 10$ (see Fig. 9 (a)) results in a small average grain size and immature microstructures, where newly introduced embryos do not have enough time to grow up. A large value of c_1 , for instance $c_1 = 100$ (see Fig. 9 (d)), leads to a relatively

large average grain size as well as long and narrow grain shapes. Fig 9 (c) is regarded as a good representative of the studied microstructure in terms of the similar average grain size and more or less equiaxed grain shapes. Hence, ' $c_1 = 50$ ' was used for the rest of the simulations.

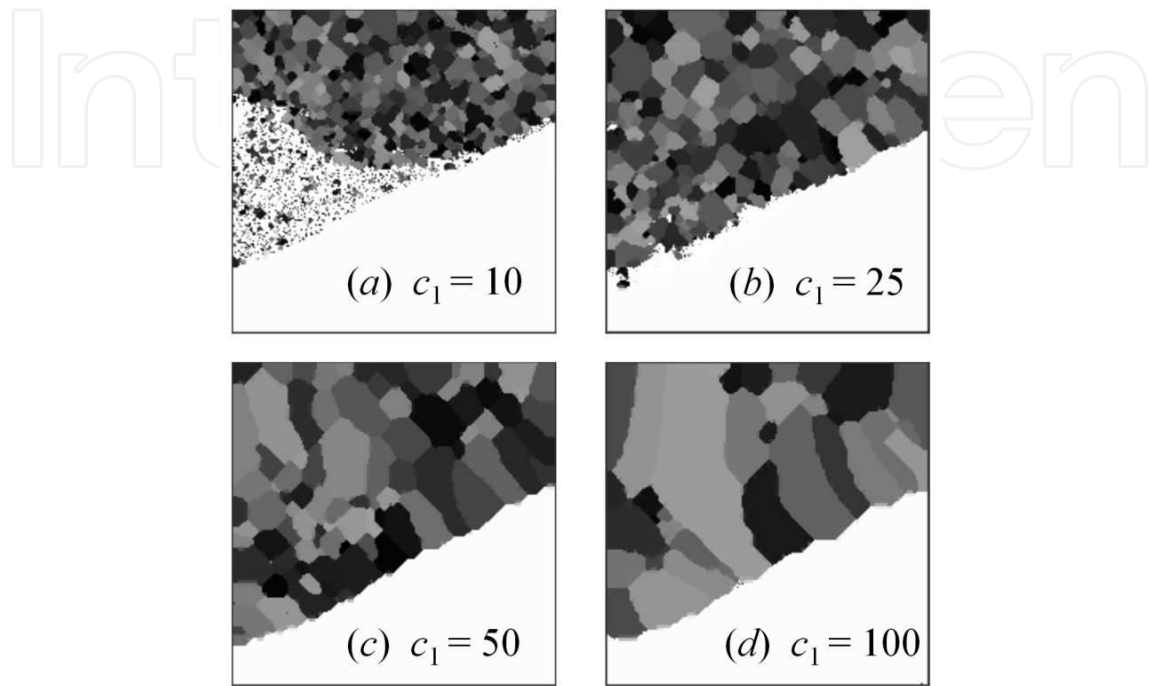


Figure 9. Simulated microstructures with four typical c_1 values [39].

4.5.3. Energy scaling

In contrast to the situation in a static recrystallization process, the stored energy of the MC sites accumulates during dynamic loading. The correlation between the external work and the stored energy is discussed as follows. It is well known that a fraction of the external work, typically varying between 1% and 15%, is stored in the metallic material during deformation [58]. According to the parameter study carried out in [38] with considering the effect of recovery, the most suitable retained fraction, 5%, is used for the unrecrystallized region in the current MC simulation. Zero is assumed to be the retained fraction for the recrystallized region. This assumption is valid due to the fact that only primary recrystallization has been found in the experimental observation of solder interconnections. It should be mentioned that if non-zero retained fraction is used for the recrystallized region, the present model is capable of predicting secondary recrystallization, which may be applicable in other cases.

The energy scaling is based on the principle that the ratios of the volume stored energy to the grain boundary energy should be equated in the MC model and the physical system [51]. The driving force due to the grain boundary energy, P^{grb} , equals $\gamma/\langle r \rangle$, where γ is the grain boundary energy per unit area and $\langle r \rangle$ is the mean grain radius. Since high angle

grain boundaries are of interest to the present investigation, the value $\gamma = 0.164 \text{ J/m}^2$ is used for the high angle grain boundary energy of Sn [22].

In the MC model, the driving force due to the stored energy density is given by $P_{MC}^{vol} = H / A$, where H is the volume stored energy of a site and A is the area of that site ($A = s^2$ in the 2-D square lattice). The driving force due to the grain boundary energy is given by

$$P_{MC}^{grgr} = \frac{\gamma_{MC}}{\langle r \rangle_{MC}} = \frac{J}{s \langle r \rangle_{MC}} = \frac{J}{s \langle r \rangle} \quad (5)$$

where γ_{MC} and $\langle r \rangle_{MC}$ are the grain boundary energy per unit and the mean grain radius in the MC model, respectively. Each unlike pair of nearest neighboring sites contributes a unit of grain boundary energy J to the system. Because of the existence of the length scale factor, s , an ideal prediction should satisfy the requirement that the mean grain radiuses in the model and in the physical system are equal, $\langle r \rangle_{MC} = \langle r \rangle$.

In the physical system, the ratio of the volume stored energy to the grain boundary energy per unit volume is

$$\frac{P^{vol}}{P^{grgr}} = \frac{P^{vol} \langle r \rangle}{\gamma} \quad (6)$$

In the MC model, the ratio is given by

$$\frac{P_{MC}^{vol}}{P_{MC}^{grgr}} = \frac{H \langle r \rangle}{J s} \quad (7)$$

Equating the ratios of the model and the physical system, and rearranging, gives

$$H = \left(\frac{P^{vol} s}{\gamma} \right) J \quad (8)$$

The increment of H can be easily calculated by Eq. (8), where s and γ are known parameters. P^{vol} distribution is obtained by scaling and mapping the energy density distribution calculated by FEM onto the MC lattice. J is a unit of grain boundary energy in the MC model. It is noteworthy that the absolute value of J is not essential and knowing the ratio, H/J , is sufficient for the MC simulation.

4.6. Nucleation

Nucleation stage is very crucial for the simulation of recrystallization. The recrystallization process is modeled by introducing nuclei (small embryos with zero stored energy) into the lattice at a constant rate, i.e. continuous nucleation. According to the locations of the valid nuclei, the nucleation is non-uniform. Although the locations of nuclei are randomly chosen, the volume stored energy of the chosen sites has to be larger than the critical stored energy, H_{cr} , before the nuclei are placed in their sites. In this way, the sites with high stored energy (e.g. near interfaces, grain boundaries, and IMPs) will have a high probability of nucleation. The critical stored energy, H_{cr} , is set to be $2J$ so that a single-site isolated embryo can grow as a new grain. Detailed discussion about the critical stored energy and critical embryo size were presented in the reference [51].

4.7. Treatment of large intermetallic particles

The intermetallic particles in SnAgCu solder are mainly Cu_6Sn_5 and Ag_3Sn . The size of IMPs varies a lot and only coarse IMPs (particle size of $1\ \mu\text{m}$ or above) are studied in the MC simulation. Zener-type particle pinning is not considered in the current model for the sake of simplicity. It is believed that fine particles do not remarkably affect the distribution of stored energy within the grains; however, coarse particles exert localized stress concentrations due to the mismatch of mechanical properties and thermal expansion coefficients. The large particles have a significant influence on stimulating nucleation.

The IMPs are introduced into the MC simulation as inert particles. They are assigned an orientation different from any of the surrounding grains and are not allowed to be reoriented during the simulation. Thus, the inert particles do not grow or move. To include the IMPs in the FE model is not realistic and too computationally expensive in view of the fact that the size and shape of IMPs vary a lot and the locations of IMPs are randomly distributed in the bulk solder. Instead, the size of the particle-affected deformation region is estimated and an energy amplification factor (EAF) distribution is introduced in order to consider the effects of IMPs.

A 2-D FE simulation was carried out to study the particle-affected deformation region and the energy amplification factor distribution. The model was composed of a solder matrix ($25 \times 25\ \mu\text{m}^2$) and a round IMP (radius = $5\ \mu\text{m}$). The material properties of the relatively soft solder matrix and the hard IMP were from the reference [59]. The loading was defined by applying the displacement on the top and right edges, i.e. bi-axial tension. The von Mises stress at the edges was not influenced by the IMP, and thereby, it was defined as one unit for the sake of normalization. The calculated stress contour and the 'EAF vs. distance' curve are shown in Fig. 10. According to the FE simulation results, the following assumptions are made with the purpose of treating IMPs in the MC simulation. Within a distance of approximately one particle radius, the calculated stored energy is amplified by a certain energy amplification factor before mapped onto the Monte Carlo lattice. The EAF for the site close to the IMP is about '1.12' and the EAF decreases linearly to '1' for the site more than one radius distance away from the IMP. In order to realize this, a new matrix storing the EAF distribution is introduced to the Monte Carlo algorithm. Every time the stored energy of a site is

updated during the recrystallization simulation, the energy increment is multiplied by the associated EAF before being added to the site. By introducing the EAF, stored energy density close to IMPs is higher than usual, leading to a higher driving force for nucleation and growth of recrystallized grains. Thus, the particle stimulated nucleation is well taken into consideration in the MC simulation.

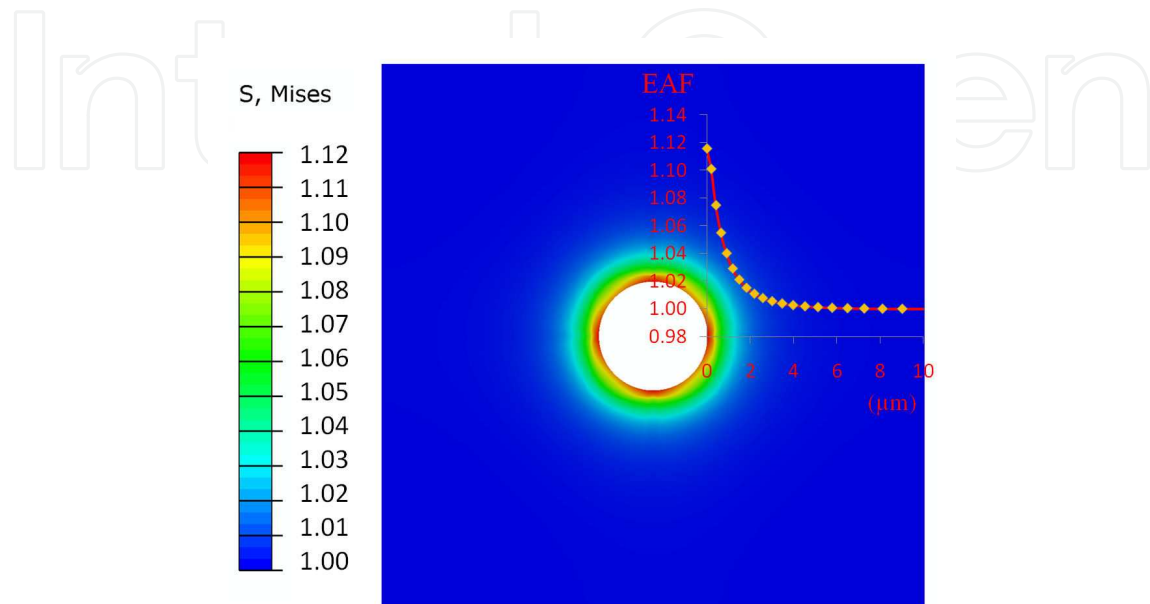


Figure 10. von Mises stress contour and 'EAF vs. distance' curve [39].

5. Simulation results and experimental verifications

5.1. Simulation with no presence of IMPs

A solder interconnection was selected to verify the performance of the presented algorithm. The interconnection was the second diagonal solder interconnection from the right end as shown in Fig. 7. The heterogeneous deformation of the interconnection after 1000 thermal cycles is shown in Fig. 11 (a). The image was taken with bright light before polishing. The persistent slip bands are visible in the image, which show the severe plastic deformation near the interface on the component side. The distribution of the heavily deformed regions agrees well with the calculated inelastic strain energy density distribution (see Fig. 11 (b)). This agreement verifies that the energy input for the microstructural simulation is valid. The dashed rectangle in Fig. 11 (b) shows the domain of the following microstructural simulation.

Different from the experimental observations, the Monte Carlo simulation results offer a continuing process of the microstructural evolution. Three snapshots from the MC simulation with a time interval, 500 thermal cycles (TCs), are shown in Fig. 12. On the left side of

the simulated microstructures, the related micrographs are presented. According to the simulation results, the incubation time for the recrystallization is about 400 TCs. During the incubation period, the stored energy is accumulated, but the magnitude remains below the critical value. As a result, no new grains are formed before 400 TCs. The upper right corner of the solder interconnection is the location where the highest inelastic strain energy is concentrated (see Fig. 11 (b)). It is this very same location where the magnitude of the stored energy first exceeds the critical value and recrystallization is initiated (see Fig. 12 (a) and Fig. 12 (d)). Then, as shown in Fig. 12 (e), the recrystallized region expands towards the lower left of the interconnection, which is in good agreement with the experimental finding (see Fig. 12 (b)). By comparing Fig. 12 (e) and 12 (f), it is found that the migration rate of the recrystallization front slows down during the period from 1000 TCs to 1500 TCs due to the decreasing driving force in the lattice. In the micrograph, Fig. 12 (c), cracks and voids are obvious, meaning that the continuity assumption of the finite element model is no longer valid. Therefore, the difference between the experimental finding and the simulated microstructure, Fig. 12 (f), is understandable. A possible solution is to simulate the behaviors of cracks and voids in the Monte Carlo model, output the microstructures to the finite element model, and then, use the calculated results as the inputs for the next round Monte Carlo simulation.

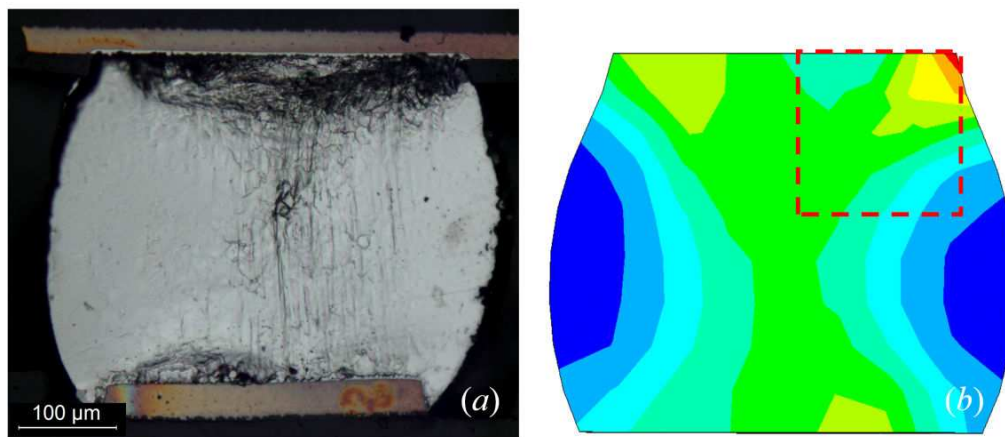


Figure 11. a) Plastic deformation of the solder interconnection after 1000 thermal cycles, (b) FEM-calculated inelastic strain energy density distribution, dashed rectangle shows the domain of the microstructural simulation [39].

5.2. Simulation with presence of IMPs

There was no obvious IMP-affected recrystallization in any of the in situ samples. Most of the observed recrystallized microstructures were located close to the interface region where the stored energy density was the highest. In order to focus on the influence of the IMPs and exclude the effects of the heterogeneous energy distribution, a uniform stored energy density distribution was assumed during the simulation. The assumption is valid when the calculation domain is located in the center part of the solder interconnection, where the energy magnitude is relatively low and energy distribution is quite uniform. Furthermore, the ener-

gy amplification factors introduced in Section 4.5.3 were used to increase the energy around the IMPs.

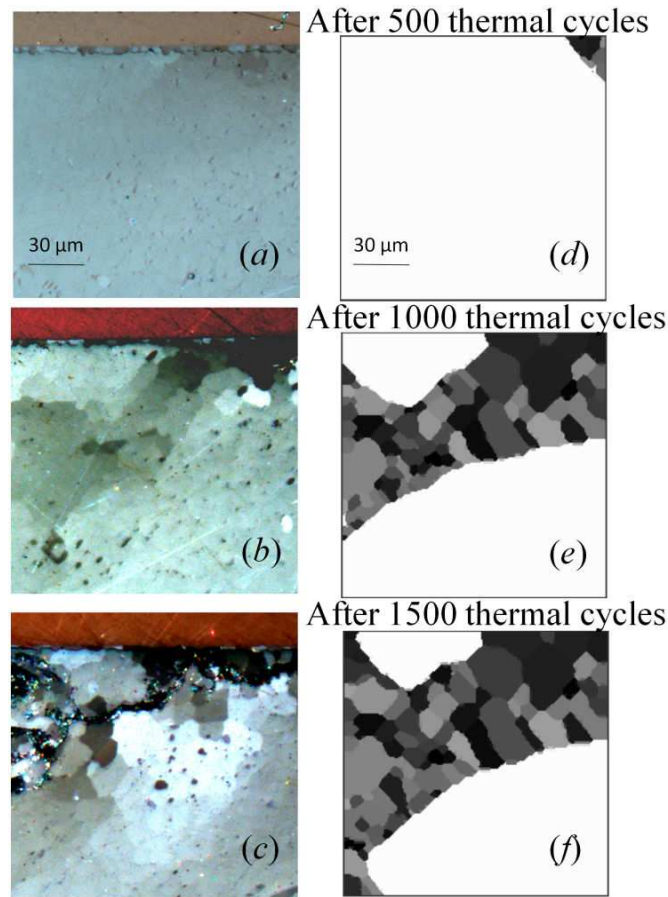


Figure 12. *a)*, *(b)*, and *(c)* are experimentally observed microstructures of the same location; *(d)*, *(e)*, and *(f)* are simulated microstructures after 500, 1000, and 1500 thermal cycles respectively [39].

A micrograph from a normal thermal cycling test was used to verify the simulation results (see Fig. 13 (a)). The sample was examined after 5000 TCs and the micrograph was taken from the center of the cross section. The major IMPs were highlighted in Fig. 13 (a) for easy recognition and Fig. 13 (b) was used as the initial microstructure for the microstructural simulation. As compared with in situ samples, solder interconnections in normal thermal cycling tests experience moderate plastic deformation, and thereby, require long incubation time for recrystallization.

Four snapshots (after 1500, 3000, 4000, and 5000 TCs respectively) of the simulated microstructural evolution are presented in Fig. 14. Since there are no interfaces and pre-existing grain boundaries in the calculation domain, the intermetallic particles are the most favorable sites for nucleation in this case. The particle stimulated nucleation is shown in the simulation results and the initiation of recrystallization near the IMPs is clearly visible in Fig. 14 (a). The growth of the new grains at the expense of the strain-hardened matrix is presented in Fig. 14 (b)-(d). After 4000 TCs, since the whole matrix is consumed by the recrystallized

grains and most of the stored energy is released, there is practically no difference between Fig. 14 (c) and Fig. 14 (d). Furthermore, it is found that the IMPs tend to be located at the grain boundaries or triple junctions of the new grains as a result of the energy minimization calculation, which is consistent with the experimental results (see Fig. 13 (a)).

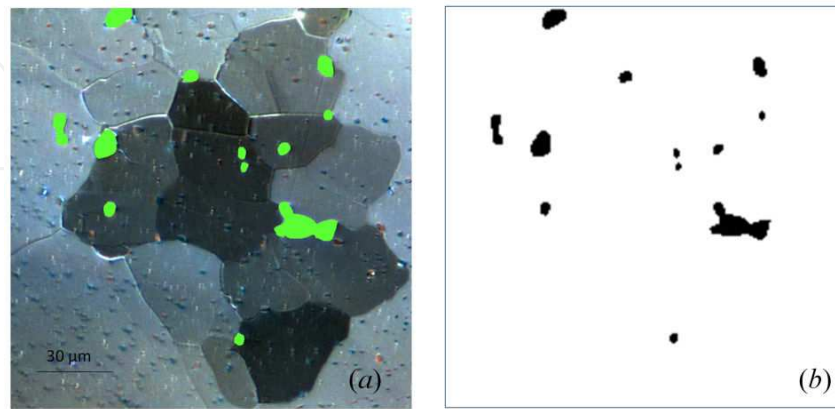


Figure 13. a) Micrograph shows IMP-affected recrystallization, (b) initial microstructure for the Monte Carlo simulation [39].

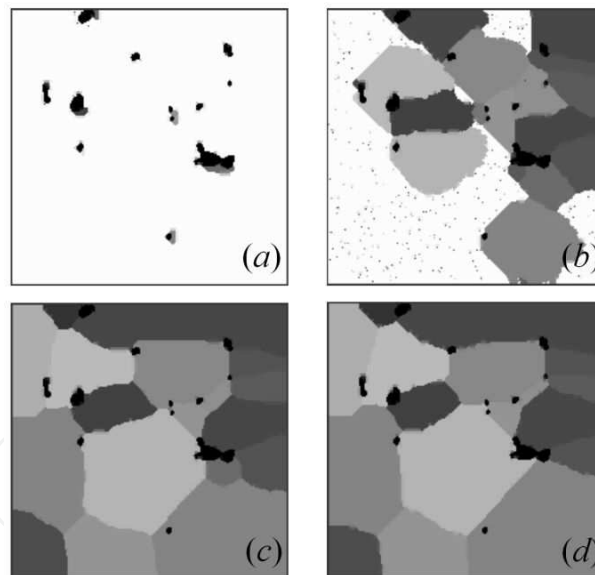


Figure 14. Simulated microstructural evolution with the presence of IMPs, (a) after 1500 TCs, (b) after 3000 TCs, (c) after 4000 TCs, (d) after 5000 TCs [39].

6. Conclusions

In this chapter, the current understanding of the microstructural changes in solder interconnections was introduced, followed by a brief review of the Monte Carlo simulations of grain

growth and recrystallization. A new algorithm for predicting dynamic recrystallization in solder interconnections during thermal cycling tests was presented. The algorithm was realized by combining a Potts model based Monte Carlo method and a finite element method. The correlation between real time and MC simulation time was established with the help of the in situ test results. Recrystallization with the presence of intermetallic particles in solder matrix was simulated by introducing the energy amplification factors in the particle-affected deformation regions. The algorithm predicts the incubation period of the recrystallization as well as the growth tendency of the recrystallized region, which are in good agreement with the experimental findings. Although the research for the microstructural simulation of solder interconnections is still at its primary stage, the presented algorithm shows potential for better reliability assessment of solder interconnections used in the electronics industry.

Acknowledgement

The authors would like to acknowledge Academy of Finland for financial support.

Author details

Jue Li, Tomi Laurila, Toni T. Mattila, Hongbo Xu and Mervi Paulasto-Kröckel

Department of Electronics, Aalto University School of Electrical Engineering, Espoo, Finland

References

- [1] R. R. Tummala, *Fundamentals of Microsystems Packaging*. New York: McGraw-Hill, 2001.
- [2] J. H. Lau (Ed.), *Solder Joint Reliability: Theory and Applications*. New York: Van Nostrand Reinhold, 1991.
- [3] J. H. Lau and Y. -H. Pao, *Solder joint reliability of BGA, CSP, flip chip, and fine pitch SMT assemblies*. New York: McGraw-Hill, 1997.
- [4] G. Q. Zhang, W. D. Van Driel, and X. J. Fan, *Mechanics of Microelectronics*. Netherlands: Springer, 2006.
- [5] J. K. Shang, Q. L. Zeng, L. Zhang, and Q. S. Zhu, "Mechanical fatigue of Sn-rich Pb-free solder alloys," *Journal of Materials Science: Materials in Electronics*, vol. 18, pp. 211-227, 2007.

- [6] E. H. Wong, S. K. W. Seah, and V. P. W. Shim, "A review of board level solder joints for mobile applications," *Microelectronics Reliability*, vol. 48, pp. 1747-1758, 2008.
- [7] Y. S. Touloukian and C. Y. Ho, *Thermal Expansion: Metallic Elements and Alloys*, New York: IFI/Plenum, 316 p, 1975.
- [8] T. T. Mattila, T. Laurila, and J. K. Kivilahti, "Metallurgical factors behind the reliability of high density lead-free interconnections," in E. Suhir, C. P. Wong, and Y. C. Lee, *Micro-and Opto-Electronic Materials and Structures: Physics, Mechanics, Design, Reliability, Packaging*, New York, Springer, pp. 313-350, 2007.
- [9] J. Karppinen, T. T. Mattila, and J. K. Kivilahti, "Formation of thermomechanical interconnection stresses in a high-end portable product," *The Proceedings of the 2nd Electronics System Integration Technology Conference*, London, UK, September 1-4, 2008, IEEE/EIA CPMT, (2008), pp. 1327-1332.
- [10] J. -P. Clech, "Acceleration factors and thermal cycling test efficiency for lead-free Sn-Ag-Cu assemblies", in *Proc SMTA International 2005*, Chicago, pp. 902-917.
- [11] R. Darveaux, "Effect of simulation methodology on solder joint crack growth correlation and fatigue life prediction", *Journal of Electronic Packaging*, vol. 124, pp. 147-154, 2002.
- [12] M. Dusek, M. Wickham, and C. Hunt, "The impact of thermal cycling regime on the shear strength of lead-free solder joints", *Soldering & Surface Mount Technology*, vol. 17, no. 2, pp. 22-31, 2005.
- [13] J. Gong, C. Liu, P. P. Conway, and V. V. Silberschmidt, "Micromechanical modelling of SnAgCu solder joint under cyclic loading: Effect of grain orientation", *Computational Materials Science*, vol. 39, pp. 187-197, 2007.
- [14] J. Li, J. Karppinen, T. Laurila, and J. K. Kivilahti, "Reliability of Lead-Free solder interconnections in Thermal and Power cycling tests", *IEEE Transactions on Components and Packaging Technologies.*, vol. 32, no. 2, pp. 302-308, 2009.
- [15] T. T. Mattila, V. Vuorinen, and J. K. Kivilahti, "Impact of printed wiring board coatings on the reliability of lead-free chip-scale package interconnections," *Journal of Materials Research*, vol. 19, no. 11, pp. 3214-3223, 2004.
- [16] G. Zeng, S. B. Xue, L. Zhang, Z. Sheng, and L. L. Gao, "Reliability evaluation of SnAgCu/SnAgCuCe solder joints based on finite element simulation and experiments", *Soldering & Surface Mount Technology*, vol. 22, no. 4, pp. 57-64, 2010.
- [17] C. J. Zhai, Sidharth, and R. Blish, "Board level solder reliability versus ramp rate and dwell time during temperature cycling", *IEEE Transactions on Device and Materials Reliability*, vol. 3, no.4, pp. 207-212, 2003.
- [18] W. Engelmaier, "Fatigue life of leadless chip carrier solder joints during power cycling," *IEEE Transactions on Components, Hybrids, and Manufacturing Technology*, vol. 6, pp. 232-237, 1983.

- [19] L. F. Coffin, "Low cycle fatigue – A review," *Applied Materials Research*, vol. 1, pp. 129-141, 1962.
- [20] R. Darveaux, "Effect of simulation methodology on solder joint crack growth correlation," *The Proceedings of the 50th Electronic Component and Technology Conference*, Chandler, AZ, May 21-24, 2000, pp. 1048-1058.
- [21] L. Zhang, S. B. Xue, L. L. Gao, Y. Chen, S. L. Yu, Z. Sheng, and G. Zeng, "Microstructure and creep properties of Sn-Ag-Cu lead-free solders bearing minor amounts of the rare earth cerium", *Soldering & Surface Mount Technology*, vol. 22, no. 2, pp. 30-36, 2010.
- [22] F. J. Humphreys and M. Hatherly, *Recrystallization and Related Annealing Phenomena*, 2nd ed., Oxford: Elsevier Ltd, 2004
- [23] R. D. Doherty, D. A. Hughes, F. J. Humphreys, J. J. Jonas, D. Juul Jensen, M. E. Kassner, W. E. King, T. R. McNelley, H. J. McQueen, and A. D. Rollett, "Current issues in recrystallization," *Materials Science and Engineering A*, 238, pp. 219 – 274, 1997.
- [24] S. Terashima, K. Takahama, M. Nozaki, and M. Tanaka, "Recrystallization of Sn grains due to thermal strain in Sn-1.2Ag-0.5Cu-0.05N solder," *Materials Transactions, Japan Institute of Metals*, vol. 45, no. 4, pp. 1383-1390, 2004.
- [25] S. Dunford, S. Canumalla, and P. Viswanadham, "Intermetallic morphology and damage evolution under thermomechanical fatigue of lead (Pb)-free solder interconnections," *The Proceedings of the 54th Electronic Components and Technology Conference*, June 1-4, 2004, Las Vegas, NV, USA, IEEE/EIA/CPMT, (2004), pp. 726-736.
- [26] J. J. Sundelin, S. T. Nurmi, and T. K. Lepistö, "Recrystallization behavior of SnAgCu solder joints," *Materials Science and Engineering A*, vol. 474, pp. 201-207, 2008.
- [27] Directive 2002/95/EC of the European Parliament and of the Council on the Restriction of the Use of Hazardous Substances in Electrical and Electronic Equipment (RoHS), Jan. 27th, 2003.
- [28] T. T. Mattila and J. K. Kivilahti, "The role of recrystallization in the failure mechanism of SnAgCu solder interconnections under thermomechanical loading," *IEEE Transactions on Components and Packaging Technologies*, vol. 33, no. 3, pp. 629-635, 2010.
- [29] A. LaLonde, D. Emelander, J. Jeannette, C. Larson, W. Rietz, D. Swenson, and D. W. Henderson, "Quantitative metallography of β -Sn dendrites in Sn_{3.8}Ag_{0.7}Cu ball grid array solder balls via electron backscatter diffraction and polarized light microscopy," *Journal of Electronic Materials*, vol. 33, no. 12, pp. 1545-1549, 2004.
- [30] D. Henderson, J. J. Woods, T. A. Gosseling, J. Bartelo, D. E. King, T. M. Korhonen, M. A. Korhonen, L. P. Lehman, E. J. Cotts, S. K. Kang, P. Lauro, D.-Y. Shih, C. Goldsmith, and K. J. Puttlitz, "The microstructure of Sn in near eutectic Sn-Ag-Cu alloy solder joints and its role in thermomechanical fatigue," *Journal of Materials Research*, vol. 19, no. 6, pp. 1608-1612, 2004.

- [31] S. Terashima and M. Tanaka, "Thermal fatigue properties of Sn-1.2Ag-0.5Cu-xNi Flip Chip interconnects," *Materials Transactions*, vol. 45, no. 3, pp. 681-688, 2004.
- [32] S. K. Kang, P. A. Lauro, D.-Y. Shih, D. W. Henderson, and K. J. Puttlitz, "Microstructure and mechanical properties of lead-free solders and solder joints used in micro-electronic applications," *IBM Journal of Research and Development*, vol. 49, no. 4/5, pp. 607-620, 2005.
- [33] A. U. Telang, T. R. Bieler, J. P. Lucas, K. N. Subramanian, L. P. Lehman, Y. Xing, and E. J. Cotts, "Grain-boundary character and grain growth in bulk tin and bulk lead-free solder alloys," *Journal of Electronic Materials*, vol. 33, no. 12, pp. 1412-1423, 2004.
- [34] L. P. Lehman, S. N. Athavale, T. Z. Fullem, A. C. Giamis, R. K. Kinyanjui, M. Lowenstein, K. Mather, R. Patel, D. Rae, J. Wang, Y. Xing, L. Zavalij, P. Borgesen, and E. J. Cotts, "Growth of Sn and intermetallic compounds in Sn-Ag-Cu solder," *Journal of Electronic Materials*, 33, 12, pp. 1429-1439, 2004.
- [35] JESD22-A104C, "Temperature Cycling," Jedec Solid State Technology Association, (2005), 16 p.
- [36] IPC-TM-650 rev. A, "Thermal Shock and Continuity, Printed Board," The Institute for Interconnecting and Packaging Electronic Circuits, (1997), 2 p.
- [37] S. Miettinen, *Recrystallization of Lead-free Solder Joints under Mechanical Load*, Master's Thesis (in Finnish), Espoo, (2005), 84 p.
- [38] J. Li, T. T. Mattila, and J. K. Kivilahti, "Multiscale simulation of recrystallization and grain growth of Sn in lead-free solder interconnections," *Journal of Electronic Materials*, vol. 39, no. 1, pp. 77-84, 2010.
- [39] J. Li, H. Xu, T. T. Mattila, J. K. Kivilahti, T. Laurila, and M. Paulasto-Kröckel, "Simulation of dynamic recrystallization in solder interconnections during thermal cycling," *Computational Materials Science*, vol. 50, pp. 690-697, 2010.
- [40] A. D. Rollett, D. J. Srolovitz, M. P. Anderson, and R. D. Doherty, "Computer simulation of recrystallization — III. Influence of a dispersion of fine particles," *Acta Metallurgica*, vol. 40, no. 12, pp. 3475-3495, 1992.
- [41] M. A. Miodownik, "A review of microstructural computer models used to simulate grain growth and recrystallisation in aluminum alloys," *Journal of Light Metals*, vol. 2, no. 3, pp. 125-135, 2002.
- [42] N. Yazdipour, C.H.J. Davies, and P.D. Hodgson, "Microstructural modeling of dynamic recrystallization using irregular cellular automata," *Computational Materials Science*, vol.44, 566-576, 2008.
- [43] A. D. Rollett and D. Raabe, "A hybrid model for mesoscopic simulation of recrystallization," *Computational Materials Science*, vol. 21, no. 1, pp. 69-78, 2001.

- [44] X. Song and M. Rettenmayr, "Modelling study on recrystallization, recovery and their temperature dependence in inhomogeneously deformed materials," *Materials Science and Engineering A*, vol. 332, no. 1-2, pp. 153-160, 2002.
- [45] Q. Yu and S. K. Esche, "A Multi-scale approach for microstructure prediction in thermo-mechanical processing of metals," *Journal of Materials Processing Technology*, vol. 169, pp. 493-502, 2005.
- [46] R. B. Potts, "Some generalized order-disorder transformations," *Proceedings of the Cambridge Philosophical Society*, vol. 48, pp. 106-109, 1952.
- [47] M. P. Anderson, D. J. Srolovitz, G. S. Grest, and P. S. Sahni, "Computer simulation of grain growth I — Kinetics," *Acta Metallurgica*, vol. 32, no. 5, pp. 783-791, 1984.
- [48] D. J. Srolovitz, M. P. Anderson, G. S. Grest, and P. S. Sahni, "Computer simulation of grain growth — III. Influence of a particle dispersion," *Acta Metallurgica*, vol. 32, no. 9, pp. 1429-1438, 1984.
- [49] A. D. Rollett, D. J. Srolovitz, and M. P. Anderson, "Simulation and theory of abnormal grain growth — Variable grain boundary energies and mobilities," *Acta Metallurgica*, vol. 37, no. 4, pp. 2127-1240, 1989.
- [50] A. D. Rollett, "Overview of modeling and simulation of recrystallization" *Progress in Materials Science*, vol. 42, no. 1-4, pp 79-99, 1997.
- [51] A. D. Rollett, P. Manohar, *Chapter 4 in Continuum Scale Simulation of Engineering Materials: Fundamentals-Microstructures-Process Applications*, ed. D. Raabe, et al., Weinheim: WILEY-VCH, 2004.
- [52] Q. Yu and S. K. Esche, "A Monte Carlo algorithm for single phase normal grain growth with improved accuracy and efficiency," *Computational Materials Science*, vol. 27, no. 3, pp. 259-270, 2003.
- [53] E. A. Holm and C. C. Battaile, "The computer simulation of microstructural evolution," *JOM*, vol. 53, no. 9, pp. 20-23, 2001.
- [54] T. O. Reinikainen, P. Marjamäki, and J. K. Kivilahti, "Deformation characteristics and microstructural evolution of SnAgCu solder joint," in *Proc. 6th EuroSim Conference*, Berlin, Germany, April, 2005, pp. 91-98.
- [55] L. Anand, "Constitutive Equations for Hot Working of Metals," *Journal of Plasticity*, vol. 1, pp. 213-231, 1985.
- [56] S. A. Safran, P. S. Sahni, and G. S. Grest, "Kinetics of ordering in two dimensions. I. Model systems," *Physical Review B*, vol. 28, no. 5, pp. 2693-2704, 1983.
- [57] D. Raabe, "Scaling Monte Carlo kinetics of the Potts model using rate theory," *Acta Materialia*, vol. 48, no. 7, pp. 1617-1628, 2000.
- [58] M. B. Bever, D. L. Holt, and A. L. Titchener, "The stored energy of cold work," *Progress in Materials Science*, vol. 17, pp.1-190, 1973.

- [59] R. R. Chromik, R. P. Vinci, S. L. Allen, and M. R. Notis, "Measuring the mechanical properties of Pb-free solder and Sn-based intermetallics by nanoindentation," *JOM*, vol. 55, no. 6, pp. 66-69, 2003.

IntechOpen

IntechOpen

